A global comparison of GEOS-Chem-predicted and remotely-sensed mineral dust aerosol optical depth and extinction profiles

Matthew S. Johnson,[1] Nicholas Meskhidze,[1] and Velayudhan Praju Kiliyanpilakkil[1]

Received 29 November 2011; revised 7 March 2012; accepted 23 May 2012; published 13 July 2012.

[1] Dust aerosol optical depth (AOD) and vertical distribution of aerosol extinction predicted by a global chemical transport model (GEOS-Chem) are compared to space-borne data from the Moderate-resolution Imaging Spectroradiometer (MODIS), Multi-Angle Imaging SpectroRadiometer (MISR), and Cloud-Aerosol Lidar and Infrared Pathfinder Satellite Observation (CALIPSO) for March 2009 to February 2010. Model-predicted and remotely-sensed AOD/aerosol extinction profiles are compared over six regions where aerosol abundances are dominated by mineral dust. Calculations indicate that over the regions examined in this study (with the exception of Middle Eastern dust sources) GEOS-Chem predicts higher AOD values compared to MODIS and MISR. The positive bias is particularly pronounced over the Saharan dust source regions, where model-predicted AOD values are a factor of 2 to 3 higher. The comparison with CALIPSO-derived dust aerosol extinction profiles revealed that the model overestimations of dust abundances over the study regions primarily occur below ~4 km, suggesting excessive emissions of mineral dust and/or uncertainties in dust optical properties. The implementation of a new dust size distribution scheme into GEOS-Chem reduced the yearly-mean positive bias in model-predicted AOD values over the study regions. The results were most noticeable over the Saharan dust source regions where the differences between model-predicted and MODIS/MISR retrieved AOD values were reduced from 0.22 and 0.17 to 0.02 and −0.04, respectively. Our results suggest that positive/negative biases between satellite and model-predicted aerosol extinction values at different altitudes can sometimes even out, giving a false impression for the agreement between remotely-sensed and model-predicted column-integrated AOD data.

Citation: Johnson, M. S., N. Meskhidze, and V. Praju Kiliyanpilakkil (2012), A global comparison of GEOS-Chem-predicted and remotely-sensed mineral dust aerosol optical depth and extinction profiles, *J. Adv. Model. Earth Syst., 4,* M07001, doi:10.1029/2011MS000109.

1. Introduction

[2] Mineral dust particles are one of the most abundant aerosols in the Earth's atmosphere. With global emission rates ~2150 Tg yr^{-1} (1 Tg = 10^{12} g) mineral dust makes up ~40% of the global annual mass of aerosols emitted from the Earth [*Forster et al.*, 2007]. These natural aerosols can directly impact radiative forcing by altering incoming solar radiation in the atmosphere through scattering and absorption [*Tegen et al.*, 1997; *Haywood and Boucher*, 2000] and indirectly by changing cloud microphysics and optical properties by acting as cloud condensation (CCN) and/or ice nuclei (IN) [*Wurzler et al.*, 2000; *Sassen et al.*, 2003; *DeMott et al.*, 2003; *Solomos et al.*, 2011]. Presently, there remains considerable uncertainty in both the sign and magnitude of the net direct radiative forcing by mineral dust, ranging from −0.56 to +0.4 W m^{-2} [*Forster et al.*, 2007]. General circulation models also provide a wide variety of estimates for the indirect radiative forcing by dust particles acting as IN with an estimated range from −1.0 to −2.1 W m^{-2} [*Lohmann and Diehl*, 2006]. Additionally, mineral dust can influence marine biogeochemical processes as the atmospheric deposition of aeolian dust is recognized as an important natural pathway for nutrient (i.e., iron (Fe) and phosphorus) deposition to the surface waters of the oceans [*Martin and Fitzwater*, 1988; *Jickells et al.*, 2005; *Meskhidze et al.*, 2005]. Mesoscale Fe enrichment experiments have shown that the supply of bioavailable iron to Fe-depleted surface waters (also known as high-nitrate low-chlorophyll (HNLC) regions) exerts control on the dynamics of plankton growth, which in turn affects the biogeochemical cycles of carbon, nitrogen, silicon, sulfur, and can ultimately influence the Earth's climate [e.g., *Boyd et al.*, 2007]. Large uncertainties in the

[1]Marine Earth and Atmospheric Science, North Carolina State University, Raleigh, North Carolina, USA.

1942-2466/12/2011MS000109

radiative forcing of mineral dust aerosols can strongly affect the model-predicted extent of human induced climate change and our ability to predict future climate. Therefore, the improved quantification of mineral dust emission rates, particle-size distributions, mixing state, chemical transformations in the atmosphere, and its CCN and IN properties are some of the main motivations of present-day research.

[3] Global atmospheric distributions of mineral dust used in radiative budget calculations and height-dependent remote sensing algorithms (i.e., UV remote sensing) are often determined using chemical transport models (CTMs) such as GEOS-Chem [*Torres et al*., 1998, 2007; *Hu et al*., 2009]. This state-of-the-art model is widely-used for the evaluation of atmospheric chemical composition, aerosol transport, aerosol optical depth (AOD), and nutrient deposition to the oceans [e.g., *Bey et al*., 2001; *Heald et al*., 2006; *van Donkelaar et al*., 2006; *Solmon et al*., 2009; *Johnson et al*., 2010, 2011]. GEOS-Chem can also be used in combination with global climate models (GCMs) to study past and future climate [e.g., *Wu et al*., 2007, 2008]. However, recent studies have reported large discrepancies between GEOS-Chem-predicted mineral dust concentrations/AODs in comparison to measurement and remotely-sensed data [*Generoso et al*., 2008; *Fairlie et al*., 2010]. For example, based on the differences between model results and measurements of Asian dust concentrations, it was suggested that when GEOS-Chem is run with GEOS-4 meteorology global emission rates of mineral dust should be reduced by a factor of two [*Fairlie et al*., 2010]. A factor of three reduction in dust emission rates was recommended for the Saharan dust sources based on the comparison of model-predicted AOD and remotely-sensed data [*Generoso et al*., 2008]. Such large uncertainties for different dust producing regions are believed to be caused by the fact that the GEOS-Chem dust mobilization scheme was developed and implemented for GEOS-3 meteorological fields. GEOS-Chem-predicted dust emissions are being driven by the "saltation" process, which is dependent to the third power of 10 m wind speed [*Zender et al*., 2003]. Therefore, small variations in surface wind speeds can lead to significant discrepancies in dust emission fluxes and total column concentrations. Higher surface winds in GEOS-4 datasets (with a global positive wind bias of 0.2 m s^{-1} between GEOS-4 and the National Centers for Environmental Prediction (NCEP) reanalysis [*Jaeglé et al*., 2011]) were suggested to cause the over-prediction of mineral dust emissions and total column concentrations in comparison to observational data [*Generoso et al*., 2008; *Fairlie et al*., 2010].

[4] Now that GEOS-Chem is run with GEOS-5 meteorological fields it is particularly important to evaluate GEOS-Chem-predicted mineral dust AOD/extinction values on a global scale for these new sets of meteorological data. A recent study by *Jaeglé et al*. [2011] showed good agreement between GEOS-5 and NCEP surface wind speed values, with a globally averaged annual bias of +0.03 m s^{-1} (GEOS-5 minus NCEP). In addition to improved representation of surface wind speeds, GEOS-5 is also a better choice for simulating aerosol vertical profiles. Due to the greater vertical resolution between the surface and 2 km (5 model layers in GEOS-4 compared to 14 in GEOS-5) and accurate representation of planetary boundary layer (PBL) mixing under all possible meteorological conditions [*Lin and McElroy*, 2010], GEOS-5 meteorological fields are expected to yield a more realistic representation of the vertical structure of mineral dust in GEOS-Chem.

[5] Past studies, evaluating the spatial and temporal abundances and variations of mineral dust aerosols in GEOS-Chem, have recommended scaling model emission fluxes by comparing model results with remotely-sensed data over and downwind from the source regions using a column-integrated AOD. However, in addition to mass loading, refractive indexes, and hygroscopic properties of aerosols, model-predicted AOD values also depend on transport and removal processes which can be influenced by the dust advection altitude [*Tegen et al*., 1996; *Chin et al*., 2002], as well as particle size distribution [*Tegen and Lacis*, 1996; *Kok*, 2011]. As aerosols above the boundary layer are less affected by wet deposition processes, particle lifetimes tend to increase with altitude [e.g., *Tegen et al*., 1996]. Due to the increase in wind speed and wind shear with height, aerosols that are transported in the free troposphere also tend to be carried longer distances than dust that remains in the boundary layer [*Prospero et al*., 1981; *Li et al*., 2008]. In addition to atmospheric transport and deposition processes, mineral dust size distribution can also affect particle single scattering albedo, extinction coefficient, and total mass of emitted aerosols, influencing aerosol optical properties [e.g., *Sokolik and Toon*, 1996; *Tegen and Lacis*, 1996; *Shell and Somerville*, 2007; *Kok*, 2011]. Therefore, good/poor agreement between model-predicted and measured/remotely-sensed AOD values cannot always be used as a base for proposed changes to the emissions scheme/rates, especially, when model-predicted and measured AOD values are compared downwind from the source regions.

[6] In this work, for the first time, we evaluate global horizontal and vertical distributions of mineral dust predicted by GEOS-Chem (driven by GEOS-5 meteorology) using remotely-sensed AOD values collected by MODIS (Moderate Resolution Imaging Spectroradiometer) and MISR (Multi-Angle Imaging SpectroRadiometer) and vertical profiles of dust aerosol extinction retrieved by CALIPSO (Cloud-Aerosol Lidar and Infrared Pathfinder Satellite Observation). Such a synergistic approach to the evaluation of model-predicted mineral dust AOD/extinction calculations helps to better constrain total column burdens of mineral dust as well as aerosol vertical distribution.

2. Methods

2.1. GEOS-Chem Simulations

[7] The global chemical transport model GEOS-Chem (v8-01-01) was applied to quantify the atmospheric transport of mineral dust and associated AOD/extinction values. Assimilated meteorological fields

from the Goddard Earth Observing System (GEOS) of the NASA Global Modeling Assimilation Office are used to drive GEOS-Chem [*Bey et al.*, 2001; *Park et al.*, 2004]. The model uses GEOS-5 meteorological fields at a $2^\circ \times 2.5^\circ$ (latitude-longitude) grid resolution and 47 vertical levels. To simulate dust mobilization, GEOS-Chem combines the Dust Entrainment and Deposition (DEAD) scheme [*Zender et al.*, 2003] with the source function used in the Goddard Chemistry Aerosol Radiation and Transport (GOCART) model [*Ginoux et al.*, 2001; *Chin et al.*, 2004]. Principal source regions are deserts or dry lakes and streambeds where alluvial deposits have accumulated. Mineral dust mobilization occurs when turbulent drag forces of the atmosphere overcome gravitational inertia and inter-particle cohesion. Once mineral dust is mobilized from the surface, the model uses four standard dust bins with diameter boundaries of 0.2–2.0, 2.0–3.6, 3.6–6.0 and 6.0–12.0 μm to simulate global dust transport and deposition [*Fairlie et al.*, 2007]. Dust removal from the atmosphere occurs through dry deposition processes such as gravitational settling [*Seinfeld and Pandis*, 1998] and turbulent dry transfer of particles to the surface [*Zhang et al.*, 2001]. Dust removal by wet deposition processes includes both convective up draft scavenging and rainout/washout from large-scale precipitation [*Liu et al.*, 2001]. An in-house version of GEOS-Chem, with a prognostic dust-Fe dissolution scheme, has been applied to simulate bioavailable Fe formation within mineral dust during atmospheric transport and deposition to the oceans [*Solmon et al.*, 2009; *Johnson et al.*, 2010, 2011].

[8] Simulated 3-D profiles of aerosols influencing the magnitude and spatial distribution of AOD include mineral dust, sulfate, sea salt, and organic and black carbon. AODs at 550 nm are derived online from simulated aerosol mass concentrations and assumed lognormal size distributions of externally mixed aerosols of different types [*Martin et al.*, 2003]. Aerosol type dependent hygroscopic growth factors and refractive indices in GEOS-Chem are taken from the Global Aerosol Data Set (GADS) [*Koepke et al.*, 1997], with updated aerosol size and optical properties from *Drury et al.* [2010]. Hygroscopic growth is calculated using GEOS-5 relative humidity fields. A standard Mie code is used to calculate optical properties for each aerosol type. Total AOD values for each vertical model layer are generated assuming an external mixture of aerosols and summed over all aerosol types [*Drury et al.*, 2008]. In the baseline GEOS-Chem model, mineral dust AOD values are calculated using seven separate dust bins with each size range having size specific optical properties. The dust mass in the smallest/sub-micron size transport bin (diameter 0.2–2.0 μm) is separated into four additional bins with effective radii of 0.15, 0.25, 0.4, and 0.8 μm. The predicted dust mass is then evenly distributed into these four sub-micron size bins and used for dust AOD calculations.

[9] Recently, *Kok* [2011] suggested that the emission of mineral dust is a scale-invariant process and offered a simple theoretical expression for the power law size distribution of emitted dust aerosols. It was suggested, that when implemented in regional and global climate models, the proposed parameterization may resolve the substantial overestimation of the emitted clay size fraction of dust commonly occurring in these models [*Kok*, 2011]. Since GEOS-Chem-predicted mineral dust AOD/concentrations have previously been found to be higher compared to remotely-sensed/measurement data [*Generoso et al.*, 2008; *Fairlie et al.*, 2010], we have carried out AOD and extinction profile calculations in GEOS-Chem by reallocating model-predicted mineral dust emissions in all dust bins using the *Kok* [2011] dust aerosol size distribution parameterization. The new size distribution predicted by the *Kok* [2011] scheme is then used during transport, deposition, and AOD calculations. In section 3.4 and 3.5 we present sensitivity calculations to assess how results from this new dust size distribution scheme compare to AOD/aerosol extinction values retrieved by satellites. All model simulations were conducted from March 2009 to February 2010.

2.2. Satellite Retrievals of Aerosol Optical Depth

[10] GEOS-Chem-predicted AOD values were compared to remotely-sensed data derived by *Terra* MISR (at 555 nm wavelength) and *Aqua* MODIS (at 550 nm wavelength) satellites. *Aqua* MODIS Deep-Blue (MODIS-DB) (550 nm) data were combined with *Aqua* MODIS data in order to retrieve AOD values over bright surfaces (i.e., desert regions) [*Hsu et al.*, 2004, 2006]. Both MISR [*Martonchik et al.*, 2004; *Kahn et al.*, 2005] and MODIS [*Remer et al.*, 2005; *Hsu et al.*, 2006; *Levy et al.*, 2007a, 2007b] remotely-sensed data have been extensively evaluated and described in past literature [e.g., *Martonchik et al.*, 1998, 2002; *Kaufman et al.*, 1997; *Tanré et al.*, 1997]. In this study we use global daily gridded quality assured (QA) AOD data from MODIS and MODIS-DB Collection 5 Level-3 at $1^\circ \times 1^\circ$ resolution and MISR Collection 4 Level-3 at $0.5^\circ \times 0.5^\circ$ resolution.

[11] While passive sensors retrieve column-integrated optical extinction for all aerosols (i.e., AOD), active sensors such as the Cloud-Aerosol Lidar with Orthogonal Polarization (CALIOP) onboard the CALIPSO satellite can explicitly separate desert dust aerosols and associated optical extinction from that produced by other aerosol subtypes remotely-sensed by CALIPSO (i.e., smoke, polluted continental, polluted dust, clean continental, and clean marine). CALIPSO can further retrieve vertically resolved aerosol types and extinction profiles and therefore, can be used to evaluate GEOS-Chem-predicted vertical distributions of mineral dust. To determine the aerosol subtypes the CALIPSO algorithm uses volume depolarization ratio, integrated attenuated backscatter, the earth surface types (land/ocean), and altitude information [*Omar et al.*, 2009; *Young and Vaughan*, 2009]. Using a cloud-aerosol discrimination (CAD) algorithm, CALIOP identified features are classified into aerosol and cloud by providing a CAD score for each vertical layer [*Liu et al.*, 2009]. The standard CAD scores for the level of confidence in the aerosol-cloud classification range from −100 to 0 for aerosols and +100 to 0 for clouds. A larger absolute value of the CAD score indicates higher confidence of the feature

classification. To extract relatively high confidence cloud free data, in this study desert dust aerosols and the corresponding extinction values are extracted using CAD scores of −70 to −100 [*Liu et al.*, 2009; *Vaughan et al.*, 2004; *Kiliyanpilakkil and Meskhidze,* 2011] for the condition when initial lidar ratio (selected based on type and subtype of the layer) is equal to the final lidar ratio (derived by applying transmittance correction to the extinction processing) (http://eosweb.larc.nasa.gov/PRODOCS/calipso/Quality_Summaries/). Polluted dust aerosols were not included in mineral dust aerosol extinction calculations due to potential contamination by smoke and sea salt (A. H. Omar, personal communications, 2011). In this study we use CALIPSO Level 2 (v3.01) profile data at a 5 km resolution.

[12] Uncertainties in CALIPSO retrievals of specific aerosol subtypes and extinction values have been previously recognized [*Winker et al.*, 2009, *Yu et al.*, 2010]. For example, the algorithm that separates specific aerosol types assumes a constant lidar ratio. In reality, lidar ratios within a given aerosol subtype can vary over 30% [*Winker et al.*, 2009; *Yu et al.*, 2010]. Such uncertainty can cause for the misclassification of aerosol subtypes and errors in aerosol extinction retrievals, particularly for strongly attenuating layers, where retrieval errors tend to accumulate toward the base of the layer [*Yu et al.*, 2010]. Additional details regarding the uncertainties in CALIPSO lidar measurements of aerosol vertical distributions can be found in *Winker et al.* [2009] and *Yu et al.* [2010].

2.3. Comparison Between GEOS-Chem and Satellite Data

[13] Remotely-sensed AOD data from MODIS and MISR were re-gridded to a 2° × 2.5° grid resolution for direct comparison to the model-predicted AODs. Vertical profiles of model-predicted mineral dust aerosol extinction values were estimated by dividing daily-averaged dust AOD output by the layer height of each one of the 47 vertical levels of GEOS-Chem. To minimize the uncertainty of satellite AOD retrievals in the vicinity of clouds where hydrated aerosols occur frequently [*Zhang et al.*, 2005; *Wen et al.*, 2006, 2007; *Koren et al.*, 2007], satellite retrievals for monthly mean AOD are weighted by the number of cloud-free pixels within each grid. To be consistent with satellite data, model-predicted monthly mean AOD data was weighted by the modeled grid column cloud fraction (*CF*) as: $AOD = \frac{1}{1-CF} \sum_{i=1}^{n} (1-CF_i) AOD_i$, where *i* represents individual days. The basic statistical parameters used during this study to compare model-predicted and remotely-sensed AOD values include the correlation coefficient (R), total bias, root mean square error (RMSE), and normalized mean bias (NMB). In order to evaluate GEOS-Chem-predicted intermittent temporal (monthly/seasonal) patterns of mineral dust emission and transport from different regions, time-series analyses were applied to monthly satellite and modeled AOD data. To minimize potential error in satellite-model inter-comparison associated with aerosols other than mineral dust, statistical analyses between GEOS-Chem-predicted and MODIS/MISR retrieved AODs were carried out over the regions where aerosol abundances are dominated by mineral dust. These areas (shown in Figure 1 and hereinafter referred to as "dusty" regions) are the regions where model-predicted mineral dust aerosols contributed > 75% of total annually-averaged AOD values. Such a percentage was chosen to considerably reduce model-predicted biases in AOD calculations caused by uncertainties in simulated aerosol species other than mineral dust.

[14] Nighttime CALIPSO dust aerosol extinction retrievals are compared directly to model-predicted dust aerosol extinction outputs when CALIPSO data are available within a GEOS-Chem grid cell. CALIPSO nighttime data are used during this study because it has been shown to have higher accuracy than that collected during the daytime [*Omar et al.*, 2009]. CALIPSO data are re-gridded vertically to match the 47 vertical levels used by GEOS-Chem. Due to CALIPSO's narrow swath, near-nadir view (~70 m), and a 16-day repeating cycle, the lidar data was seasonally- and annually-averaged to acquire a global view of aerosol distribution [*Yu et al.*, 2010]. To evaluate model-predicted dust transport heights, seasonally- and annually-averaged GEOS-Chem-simulated vertical profiles of dust aerosol extinction over each "dusty" region

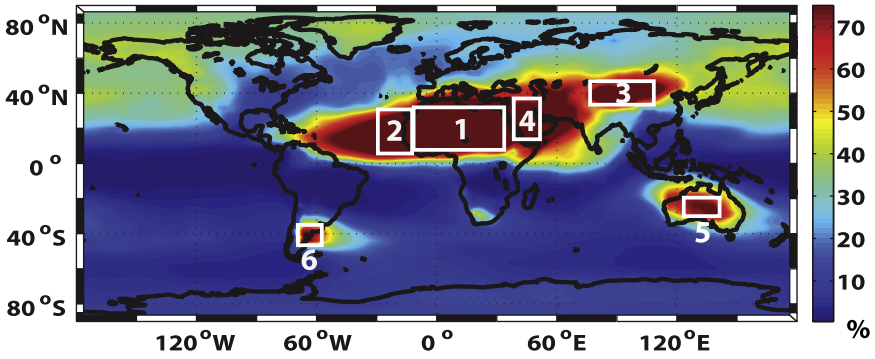

Figure 1. GEOS-Chem-predicted percent contribution of mineral dust AOD to total AOD between March 2009 and February 2010. The white boxes indicate the "dusty" regions of the 1) Saharan dust source region, 2) Saharan dust outflow (N. Atlantic Ocean), 3) Asian dust source region, 4) Middle Eastern dust source region, 5) Australian dust source region, and 6) Patagonian dust source region used for the comparison of model-predicted and remotely-sensed dust AOD/extinction values.

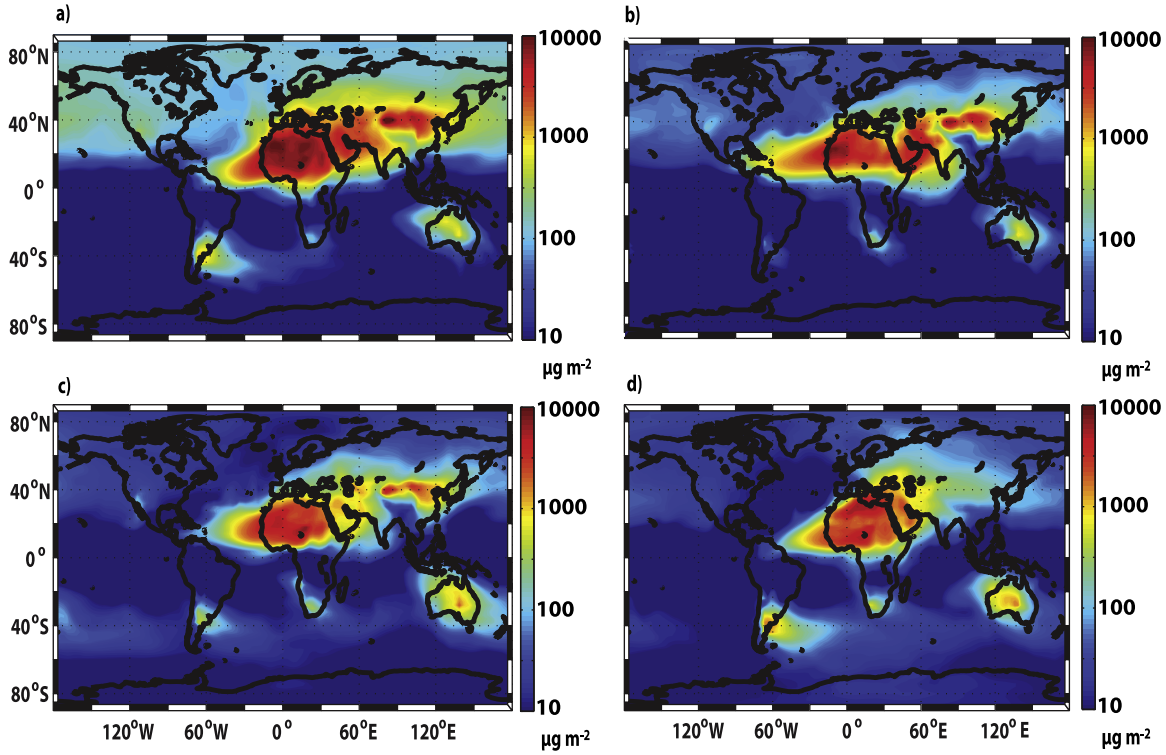

Figure 2. GEOS-Chem-predicted daily-averaged dust column burden (μg m^{-2}) during (a) March-April (MAM), (b) June-August (JJA), (c) September-November (SON), and (d) December-February (DJF).

are compared to CALIPSO-retrieved data. CALIPSO dust aerosol extinction profiles were calculated by averaging remotely-sensed dust aerosol extinction coefficients within each vertical layer of the model.

3. Results

3.1. Global Distribution of AOD Values

[15] GEOS-Chem-predicted global dust emission source regions (see Figure S1 in the auxiliary material[1]) are consistent with previous studies [e.g., *Tegen et al.*, 2002; *Prospero et al.*, 2002]. The total global annual dust emission predicted during the yearlong simulation of the current study was ~1630 Tg. This magnitude of emitted dust is within the range of dust emission fluxes predicted by global dust models considered in the recent study by *Huneeus et al.* [2011]. Figure 2 shows there are large seasonal variations in the magnitude and transport pathways of mineral dust during the simulated time period. According to this figure dust column burdens over the Sahara Desert are large year-round, with the highest concentrations associated with the deserts of north-western Sahara and the Bodélé Depression. This figure also shows that Asian dust column concentrations are particularly large during the spring season (MAM) and represent the second largest source of mineral dust globally. Dust burdens over Asia are mainly associated with the source regions of the Taklimakan and Gobi Deserts. Figure 2 shows that there is year-round dust activity over the majority of the Middle East. Total column dust concentrations over the Middle Eastern dust sources are at a maximum during the spring and summer (JJA) and at a minimum during fall (SON). In the Southern Hemisphere, the largest mineral dust column concentrations are simulated over the dust source regions of Australia and South America (see Figure 2). According to model simulations, the largest activity for Australian dust (with the source region near Lake Eyre) occurs during austral spring and summer, while South American dust sources (the Patagonia and Atacama Desert) are most active during austral summer and fall.

[16] Table 1 shows the size-resolved global emission and deposition fluxes of mineral dust predicted by the baseline GEOS-Chem model when driven by GEOS-5 meteorological fields. According to Table 1, the major fraction of model-predicted global dust mass is removed from the atmosphere through dry deposition processes. However, Table 1 also shows that dust particles between 0.2 to 3.6 μm in diameter, prone to long-range transport, are mainly removed by wet deposition processes. Overall, the GEOS-Chem-predicted global annual dust source and sink budget shown in Table 1 is comparable to past modeling studies summarized in the AeroCom phase I project [*Huneeus et al.* 2011].

[17] In general, MODIS, MISR, and GEOS-Chem give similar spatial patterns and seasonal variations of AOD values over the major global dust source regions and transport pathways (see supplementary Figure S2). However, Figure 3 shows that the model tends to predict

[1]Auxiliary materials are available in the HTML. doi:10.1029/2011MS000109

Table 1. GEOS-Chem-Predicted Global Annual Dust Sources and Sinks

Diameter Range (μm)	Emission (Tg yr^{-1})	Dry Deposition (Tg yr^{-1})	Wet Deposition (Tg yr^{-1})	Burden (Tg)
Baseline Model				
0.2–2.0	197	57	138	4.1
2.0–3.6	422	146	272	7.8
3.6–6.0	528	337	189	7.1
6.0–12.0	489	447	42	1.6
Total	1636	987	641	20.6
With Kok [2011] *Scheme*				
0.2–2.0	51	14	35	1.2
2.0–3.6	133	42	90	3.2
3.6–6.0	384	263	119	4.9
6.0–12.0	1068	994	73	7.2
Total	1636	1313	317	16.5

higher AOD values compared to remotely-sensed data over these "dusty" regions. This is particularly true over the northern Sahara Desert where, according to Figure 3, GEOS-Chem-predicted AOD values are more than a factor of 2 higher compared to both MODIS and MISR retrievals. The difference is most pronounced during MAM, one of the largest dust activity seasons for the Saharan dust sources. Over the Saharan dust outflow region of the N. Atlantic Ocean, Figure 3 shows a positive bias in model-predicted AOD values just off the coast of the continent and then a transition from warm to cool colors as the dust moves westward, suggesting that downwind from the Saharan dust source regions GEOS-Chem-predicted AOD values are lower compared to remotely-sensed data. This result is consistent with the study of *Generoso et al*. [2008], who noticed that in the model too little dust reached the Caribbean region and suggested this transition from a positive to negative bias in model-predicted AOD values could be due to the under prediction of the westward transport of mineral dust over the N. Atlantic Ocean or the over prediction of depositional fluxes [*Generoso et al*., 2008]. Figure 3 also shows some discrepancies between model-predicted and remotely-sensed AODs over the Asian dust sources, where GEOS-Chem simulated AOD values are higher in all seasons except the winter (DJF). The positive bias in the model is most noticeable during MAM when model-predicted emission rates are at a maximum. However, unlike the Saharan dust source region, where the model shows a systematic overestimation of AOD values over the entire northern Africa, larger values predicted by the model compared to satellite data are centered just above the Asian dust source regions. Over the dust source region of the Middle East, GEOS-Chem simulates lower AOD values in comparison to MODIS and MISR data. As for the Australian and Patagonian dust source regions, the comparison between model-predicted and remotely-sensed AODs is highly variable both spatially and temporally.

[18] From Figure 3 it is also apparent that GEOS-Chem displays discrepancies in predicted AOD values compared to MODIS and MISR data in regions other than ones dominated by mineral dust. For example, Figure 3 shows a persistent underestimation of AODs over marine regions as well as AOD values retrieved over the biomass burning regions of central Africa and the regions of intensive anthropogenic activities in eastern China.

3.2. Yearly-Averaged Vertical Profiles of Mineral Dust Extinction

[19] Figure 4 shows that over the "dusty" regions (with the exception of the Middle East), GEOS-Chem-predicted annually-averaged dust extinction profiles display a positive bias compared to CALIPSO retrievals. According to Figure 4 the largest discrepancies between model-predicted and satellite-retrieved dust extinction profile values were observed below 4 km height. This is particularly true over the Saharan source region, where GEOS-Chem-calculated dust aerosol extinction values are a factor of 2 to 3 higher compared to CALIPSO retrievals. Although, such discrepancies in the lower levels of the atmosphere found over the Saharan sources could be due to the strong attenuation of the CALIPSO signal by large dust plumes biasing satellite retrievals to low values [*Yu et al*., 2010], such a mechanism is highly unlikely to explain the model-satellite differences over the other "dusty" regions. Moreover, it was shown in Figure 3 that GEOS-Chem predicts higher AOD values over the Saharan dust sources compared to both MODIS and MISR satellites, therefore the model overestimation of dust extinction shown in Figure 4a is likely due to excessive emissions of mineral dust as suggested by *Generoso et al*. [2008] or uncertainties in dust optical properties (i.e., aerosol size distribution) that will be examined in section 3.4. Compared to CALIPSO retrievals GEOS-Chem-predicted dust extinction profiles over the N. Atlantic Ocean were similar to the ones over the Saharan dust source region: up to a factor of ~2 higher below 4 km and slightly lower above that height (see Figure 4b). Over the Asian dust source regions, Figure 4c reveals that the model-predicted dust extinction profile values are higher compared to CALIPSO data, with the largest discrepancy found below 4 km. This figure also reveals a consistent model over estimation of dust extinction values up to 10 km compared to remotely-sensed data. Model-predicted high altitude (above 5 km) entrainment of Asian dust is consistent with previous modeling studies suggesting that dust particles from the Taklimakan Desert can be entrained to an elevation well above 5 km and transported over long distances in the

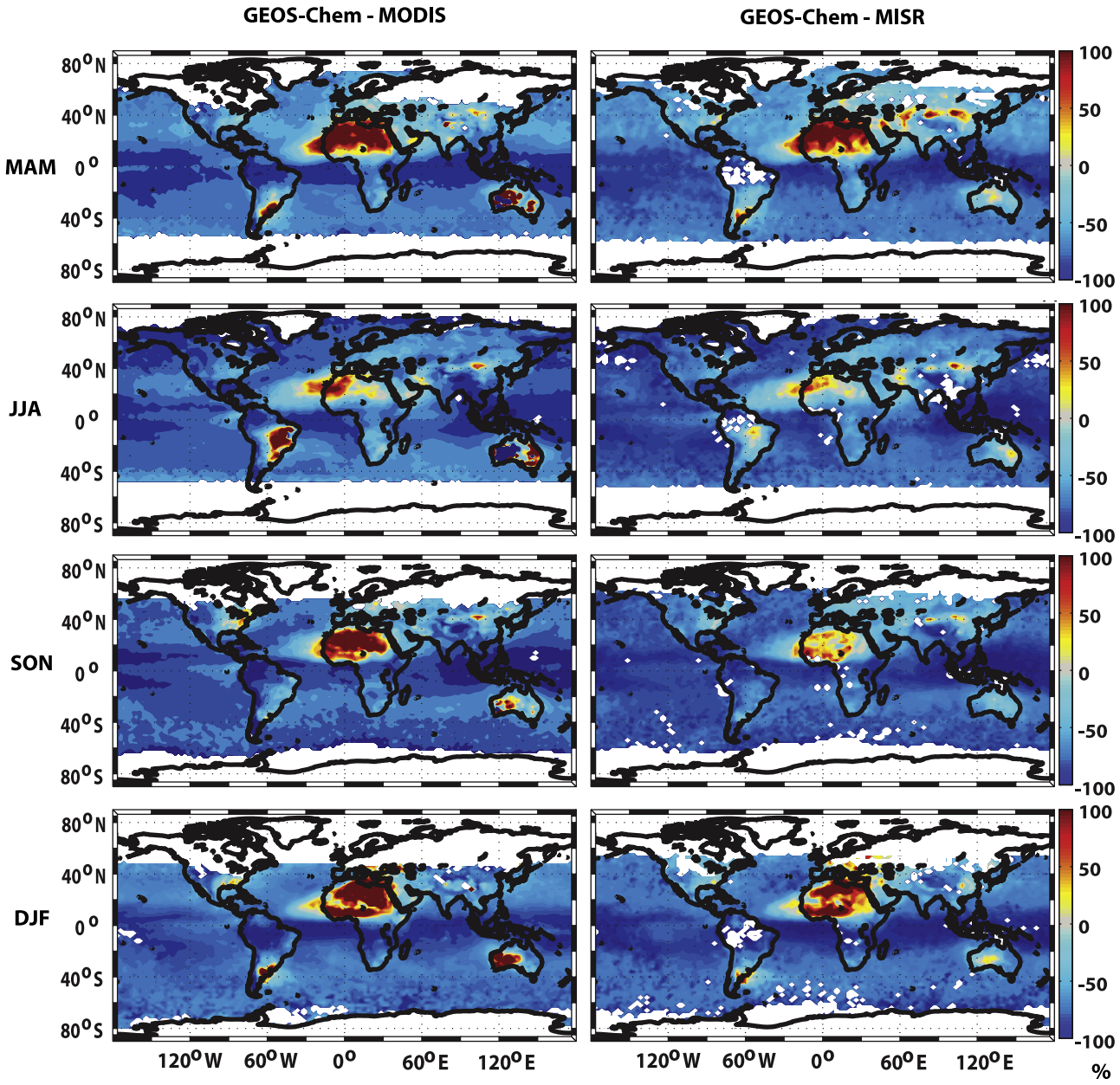

Figure 3. Seasonally-averaged percent differences for GEOS-Chem-predicted and MODIS (left) and MISR (right) retrieved AOD values.

free troposphere [*Sun et al.*, 2001; *Yu et al.*, 2010]. Possible reasons for the model-satellite differences at higher altitudes over the Asian dust sources could be related to inaccuracies in both the model-predictions and the satellite-retrievals. The possible over prediction of vertical advection of dust in GEOS-Chem combined with elevated dust concentrations over the Asian source regions may cause enhanced dust extinction values at the higher model levels. On the other hand, it is also known that CALIPSO commonly misclassifies mineral dust in the upper troposphere as thin cirrus clouds reducing dust extinction values [*Yu et al.*, 2010]. Figure 4d shows that GEOS-Chem can generally reproduce the dust extinction profiles retrieved by CALIPSO in the lower 3 km over the Middle Eastern dust source region but slightly underestimates above this height. As for the Southern Hemisphere, the model predicts higher dust extinction values compared to CALIPSO data over the desert regions of both Australia (see Figure 4e) and Patagonia (see Figure 4f) in the lower 3 km of the troposphere and displays a slight negative bias above this height.

3.3. Seasonally-Averaged Dust Extinction Profiles

[20] Figure 5 compares GEOS-Chem-predicted and CALIPSO-retrieved vertically resolved mineral dust extinction profiles for different seasons over each "dusty" region. Further details for the GEOS-Chem to CALIPSO comparison of daily mean dust extinction values for each model horizontal grid resolution and

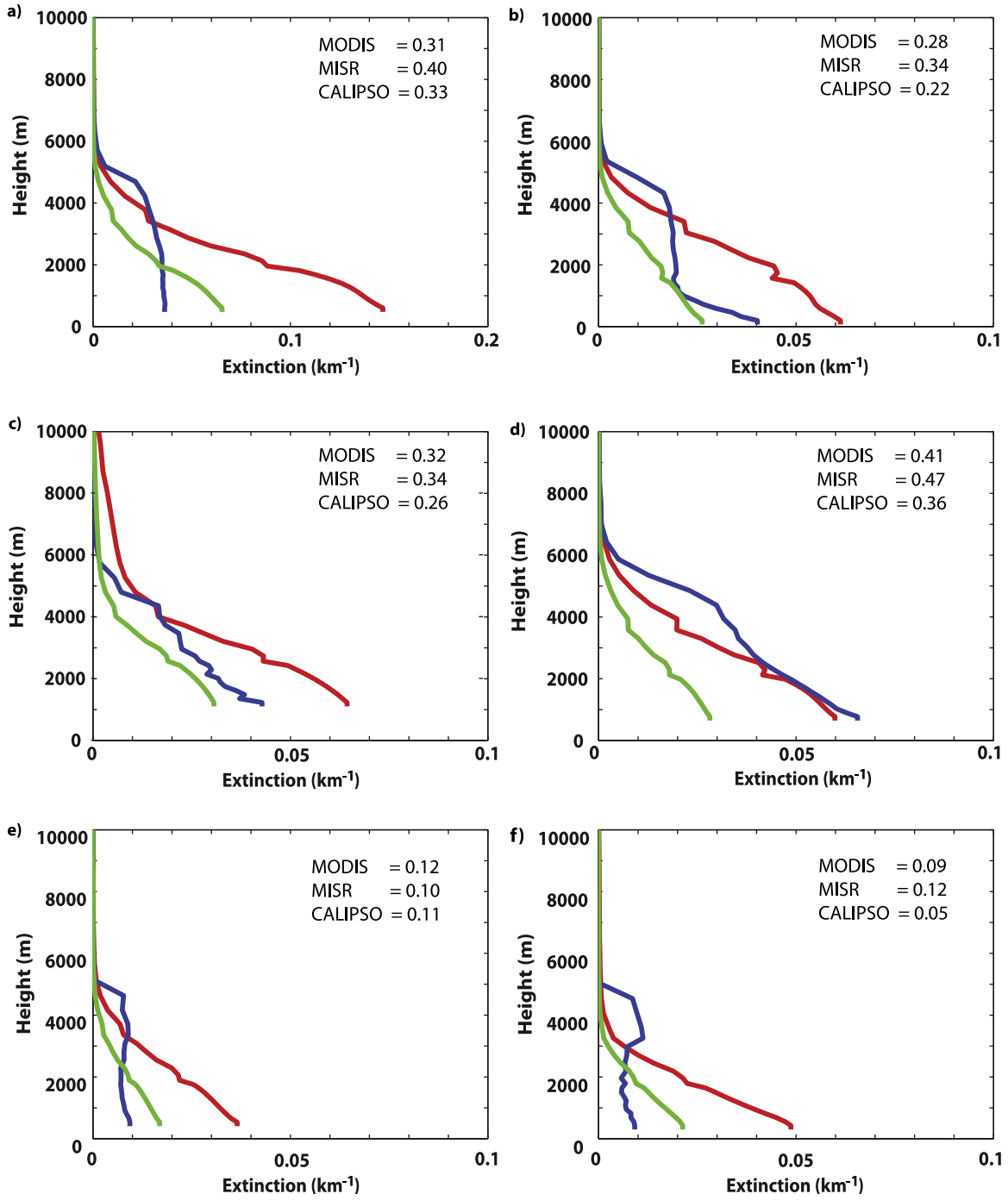

Figure 4. Annually-averaged CALIPSO-retrieved (blue line) and GEOS-Chem-simulated (standard version, red line; *Kok* [2011] scheme, green line) vertical profiles of mineral dust extinction (km^{-1}) for the (a) Saharan dust source region, (b) Saharan dust outflow region, (c) Asian dust source region, (d) Middle Eastern dust source region, (e) Australian dust source region, and (f) Patagonian dust source region. Height (m) indicates the elevation above sea level for the center of each vertical model grid. Figure insets shows regionally-averaged AOD values from MODIS, MISR, and CALIPSO.

vertical level are given in Figure S3. Figure 5a shows that over the Saharan dust source region GEOS-Chem-predicted mineral dust aerosol extinctions are generally larger in the lower troposphere (< 3 km) by well over a factor of 2. However, the comparisons between model and satellite data are reasonably good in the middle (between 3 and 6 km) and upper (> 6 km) troposphere. Model-predicted and remotely-sensed dust extinction profiles agree most closely during the summer months when both data sets suggest Saharan dust is advected to the highest altitudes during this time. Figure 5b shows that over the N. Atlantic Ocean, downwind from the

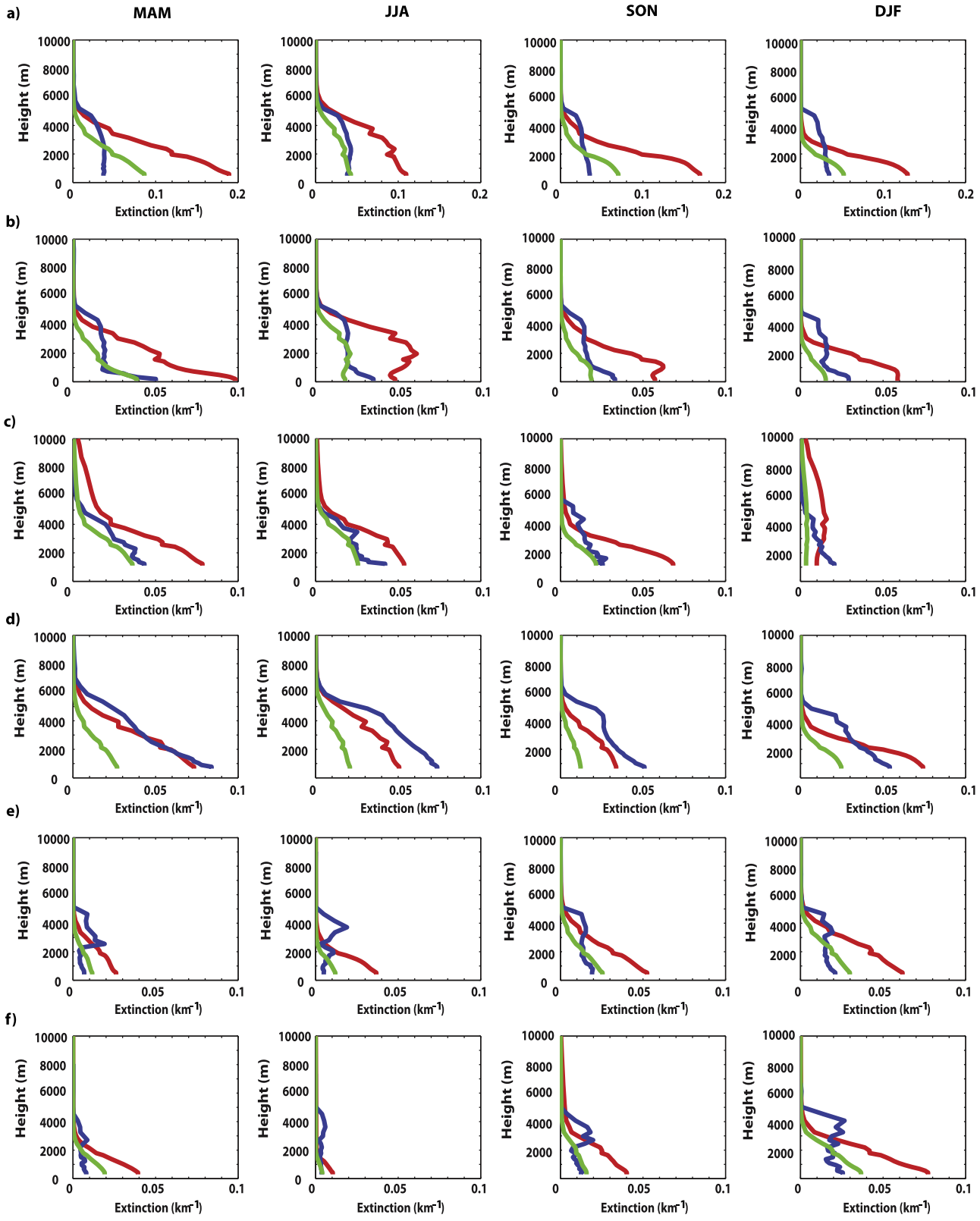

Figure 5. Seasonally-averaged CALIPSO-retrieved (blue line) and GEOS-Chem simulated (standard version, red line; *Kok* [2011] scheme, green line) vertical profiles of mineral dust extinction (km^{-1}) for the (a) Saharan dust source region, (b) Saharan dust outflow region, (c) Asian dust source region, (d) Middle Eastern dust source region, (e) Australian dust source region, and (f) Patagonian dust source region. Height (m) indicates the elevation above sea level for the center of each vertical model grid.

Saharan dust source region, model-predicted dust extinctions tend to be larger in the lower troposphere compared to CALIPSO. The simulated larger dust aerosol extinction values in this region are evident during all four seasons, but are most pronounced during the spring when model-predicted dust aerosol extinction values are highest.

[21] Figure 5c shows that over the Asian dust source regions the model predicts larger dust aerosol extinction values compared to CALIPSO data at the majority of vertical heights during all seasons. During both the winter and spring months the model tends to predict noticeably larger dust extinction values in the upper troposphere compared to remotely-sensed data. A slight negative bias in model-predicted mineral dust extinction values is also found near the surface during winter months when dust emission fluxes are at a minimum. Over the dust source region of the Middle East (see Figure 5d), model-predicted dust aerosol extinctions tend to be lower compared to CALIPSO-retrieved data. The comparison of the two data sets reveals that during spring and winter months GEOS-Chem-calculated dust extinction values are most comparable to satellite data. However, the model demonstrates a negative bias in simulated dust aerosol extinction values at all other heights and seasons. In the Southern Hemisphere, over the Australian dust source region, the model shows a tendency to predict higher values in the lower troposphere and smaller values in the upper troposphere (see Figure 5e). Over the Patagonian dust source region (see Figure 5f) GEOS-Chem produces larger values of dust aerosol extinction in the lower troposphere and smaller values in the middle and upper troposphere during all seasons when compared to CALIPSO data. Differences between model-predicted and remotely-sensed dust extinction values are most pronounced over the Patagonian dust source region during the active dust season (i.e., the austral summer).

3.4. Mineral Dust Size Distribution

[22] In this section, sensitivity calculations are presented to illustrate how GEOS-Chem-predicted AOD values and aerosol extinction profiles change when mineral dust emissions, transport, deposition, and optical properties are calculated using the dust size distribution scheme of *Kok* [2011]. Seasonally-averaged percent differences between model-predicted AOD values (with the dust aerosol size distribution scheme of *Kok* [2011]) and MODIS/MISR satellite retrievals are shown in Figure 6. The comparison of Figures 6 and 3 shows that the implementation of the *Kok* [2011] scheme led to the reduction of dust AOD values and improved agreement between model-predicted and remotely-sensed data over most of the dust producing regions. The reduction in model-predicted dust AOD values is likely due to the reallocation of the dust mass from the sub-micron mode bins to the coarse mode bins (see Table 1). Since sub-micron size dust particles tend to have higher mass extinction efficiencies, such changes in aerosol mass-size distribution led to reduced AOD values. Table 1 also shows that the reallocation of mineral dust mass to the larger transport size bins led to a decrease in atmospheric dust burden. The smaller magnitude of mineral dust mass in the atmosphere causes some further reduction in dust AOD values. The decrease in AOD values due to the new dust size distribution scheme did, however, increase the negative bias between GEOS-Chem and remotely-sensed data over the dust source region of the Middle East.

[23] Figure 4 shows that the implementation of the *Kok* [2011] dust size distribution scheme also improved the comparison between CALIPSO-derived and GEOS-Chem-predicted dust aerosol extinction profiles. However, this figure also shows that despite considerable improvements, some discrepancies remain between GEOS-Chem-predicted and CALIPSO-retrieved vertical profiles of aerosol extinction. Overall, the implementation of the *Kok* [2011] mineral dust size distribution scheme resulted in a systematic reduction in model-predicted dust extinction values at all vertical levels without reducing the overall magnitude of emitted dust (see Figure 4). Such reductions yield considerable improvement between GEOS-Chem and CALIPSO AOD/aerosol extinction data over all the "dusty" regions with the exception of the Middle East. Additional details for the comparison of dust extinction values predicted by GEOS-Chem, with the *Kok* [2011] scheme, to CALIPSO-retrieved data are given in Figure S4. Each individual data point on these scatter plots correspond to a daily mean dust aerosol extinction at a given horizontal grid resolution and vertical level within each "dusty" region. To better quantify the differences in model-predicted and remotely-sensed AOD values for the baseline simulations and the ones conducted using the *Kok* [2011] mineral dust size distribution scheme, a statistical analysis of monthly-averaged column AOD values is carried out in section 3.5.

3.5. Statistical Analysis of AOD Values

[24] Table 2 shows that when the baseline GEOS-Chem model is compared to MODIS and MISR retrievals, model-predicted regionally-averaged positive biases over the Sahara source region are 0.22 (+70%) and 0.17 (+43%), respectively. Downwind from the Sahara Desert, over the N. Atlantic Ocean, GEOS-Chem also predicts larger AOD values in comparison to MODIS and MISR data. Table 2 shows that monthly-averaged AOD values calculated by GEOS-Chem over the Sahara Desert are well correlated with remotely-sensed data with the linear correlation coefficient > 0.8, suggesting that the model can largely predict the temporal variation of mineral dust emissions from the source region. Model-predicted and remotely-sensed AOD values are also highly correlated over the N. Atlantic Ocean. The implementation of the *Kok* [2011] scheme greatly reduced the bias between model-predicted and remotely-sensed AOD values (0.02 and -0.04 for MODIS and MISR, respectively) over the Sahara Desert (see Table 2). The rest of the parameters, such as the RMSE and the NMB have also been improved. Sensitivity calculations show that downwind from the Saharan dust source region the *Kok* [2011] scheme improved the correlation between modeled and MODIS satellite data and reduced the absolute value in

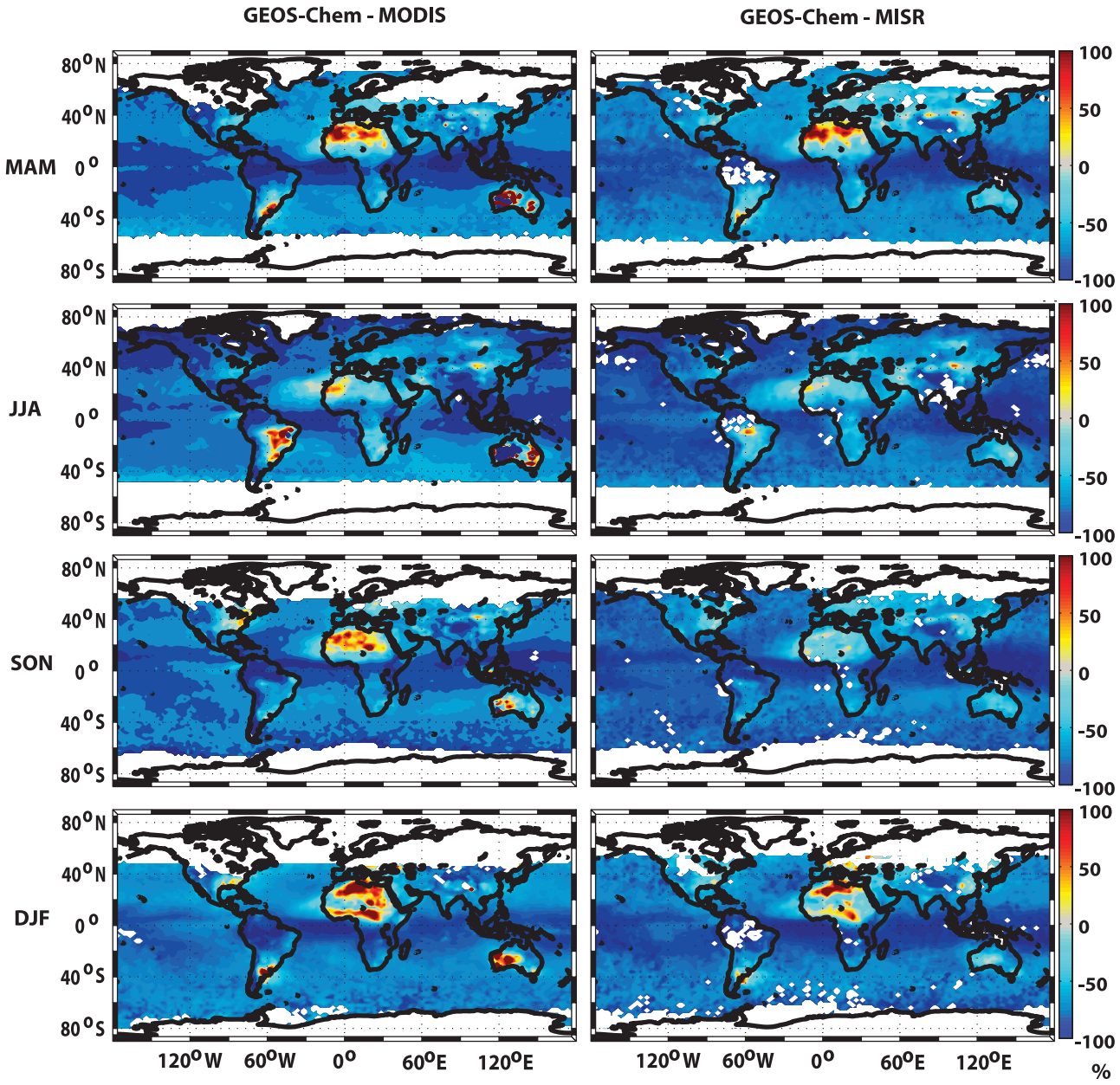

Figure 6. Seasonally-averaged percent differences for GEOS-Chem-predicted and MODIS (left) and MISR (right) AOD values. GEOS-Chem dust AODs are calculated using the size distribution parameterization of *Kok* [2011].

model bias, RMSE, and NMB in comparison to MODIS. The comparison of GEOS-Chem-predicted AOD values to MISR-retrievals yield slightly different results. The implementation of the *Kok* [2011] dust size distribution scheme improved model-satellite AOD correlation and RMSE values over the N. Atlantic Ocean, but increased model bias and NMB.

[25] High correlations between baseline model-predicted and remotely-sensed monthly AOD values (R = ~0.75 for MODIS and R = ~0.80 for MISR) over the dust source regions of Asia (see Table 2) also indicate that the model can reproduce the temporal variability of mineral dust emission and transport from the Asian dust sources. However, Table 2 shows that GEOS-Chem displays a positive bias in simulated AOD values in comparison to remotely-sensed data, particularly when compared to MISR retrievals (NMB ~30%). The implementation of the *Kok* [2011] scheme improved all statistical parameters when comparing GEOS-Chem-predicted AOD values to MISR data. In comparison to MODIS AOD values, the implementation of the new dust size distribution scheme improved the correlation and RMSE, but slightly increased the absolute value of biases and NMB.

[26] Table 2 shows that baseline model-predicted AOD values over the dust source region of the Middle East tend to display negative biases in comparison to remotely-sensed data. The possible reason for this negative bias could be the under-prediction of dust emissions from the Middle East, errors in simulated north African

Table 2. Monthly-Averaged GEOS-Chem-Predicted AOD in Comparison to MODIS and MISR Data Between March 2009 and February 2010

	MODIS				MISR			
	R	Bias	RMSE	NMB[a]	R	Bias	RMSE	NMB[a]
Baseline Model								
Sahara Source	0.86	0.22	0.29	70.1	0.88	0.17	0.24	43.2
N. Atlantic Ocean	0.79	0.07	0.15	25.5	0.85	0.04	0.14	12.5
Asian Source	0.75	0.05	0.14	13.3	0.78	0.08	0.17	31.7
Middle East	0.85	−0.12	0.16	−27.3	0.79	−0.11	0.17	−24.2
Australia	0.84	0.02	0.06	18.6	0.77	0.02	0.06	17.3
Patagonia	0.88	0.02	0.08	15.5	0.74	0.03	0.08	30.6
With Kok [2011] *Scheme*								
Sahara Source	0.90	0.02	0.10	4.95	0.85	−0.04	0.10	−11.2
N. Atlantic Ocean	0.84	−0.05	0.11	−17.5	0.90	−0.08	0.10	−24.1
Asian Source	0.82	−0.06	0.11	−17.9	0.80	−0.01	0.10	−0.20
Middle East	0.86	−0.24	0.25	−54.1	0.84	−0.25	0.26	−55.6
Australia	0.87	−0.01	0.04	−13.5	0.79	−0.01	0.04	−14.3
Patagonia	0.87	−0.01	0.05	−11.4	0.75	0.01	0.05	−0.30

[a]NMB (normalized mean bias) is in percent.

dust transport and deposition processes, and errors in anthropogenic emission inventories over this region. As expected the implementation of the *Kok* [2011] scheme reduced mineral dust AOD values even further, producing larger discrepancies between model-predicted and remotely-sensed AOD values. In the Southern Hemisphere, the baseline GEOS-Chem model simulates higher AOD values in comparison to MODIS and MISR data over both the Australian and Patagonian dust source regions. In these regions the implementation of the *Kok* [2011] dust size distribution scheme had a minimal influence on the model-satellite correlation and resulted in better agreement and improvement in all other statistical parameters in comparison to remotely-sensed data.

4. Conclusion

[27] Mineral dust AOD/extinction values predicted by the global 3-D chemical transport model GEOS-Chem were evaluated against space-borne data from MODIS, MISR, and CALIPSO. In order to minimize the contribution from aerosols other than mineral dust, six major dust source regions and transport pathways were identified. Model runs were conducted from March 2009 to February 2010. Spatial and temporal variability of seasonally- and annually-averaged horizontal profiles of AODs predicted by GEOS-Chem were comparable to remotely-sensed data by MODIS and MISR satellites. However, noticeable discrepancies between model-predicted and remotely-sensed AODs were also detected over the majority of "dusty" regions where GEOS-Chem simulates higher AOD values in compared to remotely-sensed data. The discrepancies between model-predicted AOD values and satellite retrievals were particularly pronounced over the Saharan dust source region where GEOS-Chem results were more than a factor of 2 higher compared to MODIS and MISR. The comparison of model-predicted vertical profiles of mineral dust aerosol extinction with CALIPSO retrievals revealed that over all "dusty" regions (with the exception of the Middle East) the model generally predicted larger dust aerosol extinction values compared to CALIPSO data. Furthermore, our analysis showed that discrepancies between model-predicted and remotely-sensed aerosol extinction values depend on seasonality and location. Such analysis shows the great advantage of using vertically resolved aerosol extinction profiles for model evaluation and indicates that the understanding of physical processes influencing spatiotemporal distribution of dust is necessary for improved representation of mineral aerosols in GEOS-Chem. The comparison between model-predicted and remotely-sensed dust AOD/extinctions also indicated that when AOD values are compared, positive/negative biases between satellite and model-predicted aerosol extinction values at different altitudes can sometimes even out, giving a false impression for the agreement between remotely-sensed and model-predicted aerosol data.

[28] Sensitivity calculations suggest that changing the dust mass size distribution according to the *Kok* [2011] scheme greatly reduced model-predicted positive biases in AOD values over the majority of dust source regions, particularly over the Sahara Desert. It is important to note that unlike previous studies that recommended a factor of 2 to 3 reduction of global mineral dust emissions, improvements in model-satellite AOD comparison were achieved with the implementation of the *Kok* [2011] dust mass size distribution scheme (without reducing global dust emission rates). The analysis of GEOS-Chem-predicted and CALIPSO-retrieved dust extinction profiles further showed that the *Kok* [2011] scheme improves the agreement for mineral dust extinctions over the majority of "dusty" regions.

[29] Our analysis shows that the implementation of the *Kok* [2011] dust size distribution scheme yields improved agreement between GEOS-Chem-predicted and CALIPSO-retrieved dust extinction values, however, the degree of improvement differed between "dusty" regions and time periods, suggesting that although the size distribution seems to play a key role in mineral dust AOD/extinction calculations, other factors may also influence mineral dust optical properties and light extinction. Several factors for the model-satellite discrepancies

related to GEOS-Chem are: dust emission rates, deposition fluxes, wind fields, mixing states, surface properties, assumed optical properties (i.e., extinction coefficients), and cloud and precipitation fields. Possible reasons for the discrepancies linked to CALIPSO satellite include misclassification of mineral dust in the upper troposphere as thin cirrus clouds, attenuation of signal by highly concentrated dust plumes, and the 16-day repeating cycle making it possible to obtain a global view of aerosol by averaging cloud-free profiles collected over a period of time (e.g., a season). Some of the uncertainties associated with MODIS and MISR AOD retrievals are related to instrument calibration, cloud-masking of thin cirrus clouds, assumptions of surface reflectance, aerosol shape, and aerosol model selection. Although all these factors can potentially cause model biases in calculating dust AOD/extinction values when compared to the satellite data, our calculations suggest that better representation of mineral dust aerosol optical properties can be achieved in GEOS-Chem by improving the size distribution of emitted dust aerosols.

[30] **Acknowledgments.** This research was supported by the National Science Foundation through the grant ATM-0826117 and by the National Aeronautics and Space Administration (NASA) through grant NNX11AG72G. The authors would like to thank Yongxiang Hu and Ali Omar of the NASA Langley Research Center for their help with the processing and application of CALIPSO data. Thanks are also due to Daniel Jacob and the Harvard University Atmospheric Chemistry Modeling Group for providing the baseline GEOS-Chem model used during our research. The authors would also like to thank the reviewers for their comments/recommendations as they led to improvements in the manuscript.

References

Bey, I., D. J. Jacob, R. M. Yantosca, J. A. Logan, B. Field, A. M. Fiore, Q. Li, H. Liu, L. J. Mickley, and M. Schultz (2001), Global modeling of tropospheric chemistry with assimilated meteorology: Model description and evaluation, *J. Geophys. Res.*, *06*, 23,073–23,095, doi:10.1029/2001JD000807.

Boyd, P. W., et al. (2007), Mesoscale iron enrichment experiments 1993–2005: Synthesis and future directions, *Science*, *315*, 612–617, doi:10.1126/science.1131669.

Chin, M., P. Ginoux, S. Kinne, O. Torres, B. Holben, B. Duncan, R. Martin, J. Logan, A. Higurashi, and T. Nakajima (2002), Tropospheric aerosol optical thickness from the GOCART model and comparisons with satellite and sun photometer measurements, *J. Atmos. Sci.*, *59*, 461–483, doi:10.1175/1520-0469(2002)059<0461:TAOTFT>2.0.CO;2.

Chin, M., A. Chu, R. Levy, L. Remer, Y. Kaufman, B. Holben, T. Eck, P. Ginoux, and O. Gao (2004), Aerosol distribution in the Northern Hemisphere during ACE-Asia: Results from global model, satellite observations, and Sunphotometer measurements, *J. Geophys. Res.*, *109*, D23S90, doi:10.1029/2004JD004829.

DeMott, P. J., K. Sassen, M. R. Poellet, D. Baumgardner, D. C. Rogers, S. D. Brooks, A. J. Prenni, and S. M. Kreidenweis (2003), African dust aerosols as atmospheric ice nuclei, *Geophys. Res. Lett.*, *30*(14), 1732, doi:10.1029/2003GL017410.

Drury, E., D. J. Jacob, J. Wang, R. J. D. Spurr, and K. Chance (2008), Improved algorithm for MODIS satellite retrievals of aerosol optical depths over land, *J. Geophys. Res.*, *113*, D16204, doi:10.1029/2007JD009573.

Drury, E., D. J. Jacob, R. J. D. Spurr, J. Wang, Y. Shinozuka, B. E. Anderson, A. D. Clarke, J. Dibb, C. McNaughton, and R. Weber (2010), Synthesis of satellite (MODIS), aircraft (ICARTT), and surface (IMPROVE, EPA-AQS, AERONET) aerosol observations over eastern North America to improve MODIS aerosol retrievals and constrain surface aerosol concentrations and sources, *J. Geophys. Res.*, *115*, D14204, doi:10.1029/2009JD012629.

Fairlie, T. D., D. J. Jacobs, and R. J. Rokjin (2007), The impact of transpacific transport of mineral dust in the United States, *Atmos. Environ.*, *41*, 1251–1266, doi:10.1016/j.atmosenv.2006.09.048.

Fairlie, T. D., D. J. Jacob, J. E. Dibb, B. Alexander, M. A. Avery, A. van Donkelaar, and L. Zhang (2010), Impact of mineral dust on nitrate, sulfate, and ozone in transpacific Asian pollution plumes, *Atmos. Chem. Phys.*, *10*, 3999–4012, doi:10.5194/acp-10-3999-2010.

Forster, P. et al. (2007), Changes in atmospheric constituents and radiative forcing, in *Climate Change 2007: The Physical Science Basis: Working Group I Contribution to the Fourth Assessment Report of the IPCC*, edited by S. Solomon et al., chap. 2, pp. 131–234, Cambridge Univ. Press, Cambridge, U. K.

Generoso, S., I. Bey, M. Labonne, and F. M. Breon (2008), Aerosol vertical distribution in dust outflow over the atlantic: Comparisons between GEOS-chem and cloud-aerosol lidar and infrared pathfinder satellite observation (CALIPSO), *J. Geophys. Res.*, *113*, D24209, doi:10.1029/2008JD010154.

Ginoux, P., M. Chin, I. Tegen, J. M. Prospero, B. Holben, O. Dubovik, and S.-J. Lin (2001), Sources and distributions of dust aerosols simulated with the GOCART model, *J. Geophys. Res.*, *106*, 20,255–20,273, doi:10.1029/2000JD000053.

Haywood, J., and O. Boucher (2000), Estimates of the direct and indirect radiative forcing due to tropospheric aerosols, *Rev. Geophys.*, *38*, 513–543, doi:10.1029/1999RG000078.

Heald, C. L., D. J. Jacob, R. J. Park, B. Alexander, T. D. Fairlie, R. M. Yantosca, and D. A. Chu (2006), Transpacific transport of Asian anthropogenic aerosols and its impact on surface air quality in the United States, *J. Geophys. Res.*, *111*, D14310, doi:10.1029/2005JD006847.

Hsu, N. C., S. C. Tsay, M. D. King, and J. R. Herman (2004), Aerosol properties over bright-reflecting source regions, *IEEE Trans. Geosci. Remote Sens.*, *42*, 557–569, doi:10.1109/TGRS.2004.824067.

Hsu, N. C., S. C. Tsay, M. D. King, and J. R. Herman (2006), Deep blue retrievals of Asian aerosol properties during ACE-Asia, *IEEE Trans. Geosci. Remote Sens.*, *44*, 3180–3195, doi:10.1109/TGRS.2006.879540.

Hu, R.-M., R. S. Sakhi, and B. E. A. Fisher (2009), New algorithms and their application for satellite remote sensing of surface $PM_{2.5}$ and aerosol absorption, *J. Aerosp. Sci.*, *40*, 394–402, doi:10.1016/j.jaerosci.2009.01.005.

Huneeus, N., et al. (2011), Global dust model intercomparison in AeroCom phase I, *Atmos. Chem. Phys.*, *11*, 7781–7816, doi:10.5194/acp-11-7781-2011.

Jaeglé, L., P. K. Quinn, T. Bates, B. Alexander, and J.-T. Lin (2011), Global distribution of sea salt aerosols: New constraints from in situ and remote sensing observations, *Atmos. Chem. Phys.*, *10*, 25,687–25,742.

Jickells, T. D., et al. (2005), Global iron connections between desert dust, ocean biogeochemistry, and climate, *Science*, *308*, 67–71, doi:10.1126/science.1105959.

Johnson, M. S., N. Meskhidze, F. Solmon, S. Gassó, P. Y. Chuang, D. M. Gaiero, R. M. Yantosca, S. Wu, Y. Wang, and C. Carouge (2010), Modeling dust and soluble iron deposition to the South Atlantic Ocean, *J. Geophys. Res.*, *115*, D15202, doi:10.1029/2009JD013311.

Johnson, M. S., N. Meskhidze, V. P. Kiliyanpilakkil, and S. Gassó (2011), Understanding the transport of Patagonian dust and its influence on marine biological activity in the South Atlantic Ocean, *Atmos. Chem. Phys.*, *11*, 2487–2502, doi:10.5194/acp-11-2487-2011.

Kahn, R. A., B. J. Gaitley, J. V. Martonchik, D. J. Diner, K. A. Crean, and B. Holben (2005), Multiangle Imaging Spectroradiometer (MISR) global aerosol optical depth validation based on 2 years of coincident Aerosol Robotic Network (AERONET) observations, *J. Geophys. Res.*, *110*, D10S04, doi:10.1029/2004JD004706.

Kaufman, Y. J., D. Tanré, L. A. Remer, E. Vermote, A. Chu, and B. N. Holben (1997), Operational remote sensing of tropospheric aerosol over land from EOS moderate resolution imaging spectroradiometer, *J. Geophys. Res.*, *102*, 17,051–17,067, doi:10.1029/96JD03988.

Kiliyanpilakkil, V. P., and N. Meskhidze (2011), Deriving the effect of wind speed on clean marine aerosol optical properties using the A-Train satellites, *Atmos. Chem. Phys.*, *11*, 11,401–11,413, doi:10.5194/acp-11-11401-2011.

Koepke, P., M. Hess, I. Schult, and E. P. Shettle (1997), Global aerosol data set, *Rep. 243*, Max-Planck Inst. fur Meteorol., Hamburg, Germany.

Kok, J. F. (2011), A scaling theory for the size distribution of emitted dust aerosols suggests climate models underestimate the size of the

global dust cycle, *Proc. Natl. Acad. Sci. U. S. A.*, *108*(3), 1016–1021, doi:10.1073/pnas.1014798108.

Koren, I., L. A. Remer, Y. J. Kaufman, Y. Rudich, and J. V. Martins (2007), On the twilight zone between clouds and aerosols, *Geophys. Res. Lett.*, *34*, L08805, doi:10.1029/2007GL029253.

Levy, R. C., L. A. Remer, and O. Dubovik (2007a), Global aerosol optical properties and application to MODIS aerosol retrieval over land, *J. Geophys. Res.*, *112*, D13210, doi:10.1029/2006JD007815.

Levy, R. C., L. A. Remer, S. Mattoo, E. Vermote, and Y. J. Kaufman (2007b), Second-generation algorithm for retrieving aerosol properties over land from MODIS spectral reflectance, *J. Geophys. Res.*, *112*, D13211, doi:10.1029/2006JD007811.

Li, F., P. Ginoux, and V. Ramaswamy (2008), Distribution, transport, and deposition of mineral dust in the Southern Ocean and Antarctica: Contribution of major sources, *J. Geophys. Res.*, *113*, D10207, doi:10.1029/2007JD009190.

Lin, J.-T., and M. McElroy (2010), Impacts of boundary layer mixing on pollutant vertical profiles in the lower troposphere: Implications to satellite remote sensing, *Atmos. Environ.*, *44*(14), 1726–1739, doi:10.1016/j.atmosenv.2010.02.009.

Liu, H., D. J. Jacob, I. Bey, and R. M. Yantosca (2001), Constraints from ^{210}Pb and ^{7}Be on wet deposition and transport in a global three-dimensional chemical tracer model driven by assimilated meteorological fields, *J. Geophys. Res.*, *106*, 12,109–12,128, doi:10.1029/2000JD900839.

Liu, Z., M. Vaughan, D. Winker, C. Kittaka, B. Getzewich, R. Kuehn, A. Omar, K. Powell, C. Trepte, and C. Hostetler (2009), The CALIPSO lidar cloud and aerosol discrimination: Version 2 algorithm and initial assessment of performance, *J. Atmos. Oceanic Technol.*, *26*, 1198–1213, doi:10.1175/2009JTECHA1229.1.

Lohmann, U., and K. Diehl (2006), Sensitivity studies of the importance of dust ice nuclei for the indirect aerosol effect on stratiform mixed-phase clouds, *J. Atmos. Sci.*, *63*, 968–982, doi:10.1175/JAS3662.1.

Martin, J. H., and S. E. Fitzwater (1988), Iron-deficiency limits phytoplankton growth in the northeast pacific subarctic, *Nature*, *331*, 341–343, doi:10.1038/331341a0.

Martin, R. V., D. J. Jacob, R. M. Yantosca, M. Chin, and P. Ginoux (2003), Global and regional decreases in tropospheric oxidants from photochemical effects of aerosols, *J. Geophys. Res.*, *108*(D3), 4097, doi:10.1029/2002JD002622.

Martonchik, J. V., D. J. Diner, R. Kahn, T. P. Ackerman, M. M. Verstraete, B. Pinty, and H. R. Gordon (1998), Techniques for the retrieval of aerosol properties over land and ocean using multi-angle imaging, *IEEE Trans. Geosci. Remote Sens.*, *36*, 1212–1227, doi:10.1109/36.701027.

Martonchik, J. V., D. J. Diner, K. A. Crean, and M. A. Bull (2002), Regional aerosol retrieval results from MISR, *IEEE Trans. Geosci. Remote Sens.*, *40*, 1520–1531, doi:10.1109/TGRS.2002.801142.

Martonchik, J. V., D. J. Diner, R. Kahn, B. Gaitley, and B. N. Holben (2004), Comparison of MISR and AERONET aerosol optical depths over desert sites, *Geophys. Res. Lett.*, *31*, L16102, doi:10.1029/2004GL019807.

Meskhidze, N., W. L. Chameides, and A. Nenes (2005), Dust and pollution: A recipe for enhanced ocean fertilization?, *J. Geophys. Res.*, *110*, D03301, doi:10.1029/2004JD005082.

Omar, A., et al. (2009), The CALIPSO automated aerosol classification and lidar ratio selection algorithm, *J. Atmos. Oceanic Technol.*, *26*, 1994–2014, doi:10.1175/2009JTECHA1231.1.

Park, R. J., D. J. Jacob, B. D. Field, R. M. Yantosca, and M. Chin (2004), Natural and transboundary pollution influences on sulfate nitrate-ammonium aerosols in the United States: Implications for policy, *J. Geophys. Res.*, *109*, D15204, doi:10.1029/2003JD004473.

Prospero, J. M., R. A. Glaccum, and R. T. Nees (1981), Atmospheric transport of soil dust from Africa to South America, *Nature*, *289*, 570–572, doi:10.1038/289570a0.

Prospero, J. M., P. Ginoux, O. Torres, and S. E. Nicholson (2002), Environmental characterization of global sources of atmospheric soil dust identified with the Nimbus 7 Total Ozone Mapping Spectrometer (TOMS) absorbing aerosol product, *Rev. Geophys.*, *40*(1), 1002, doi:10.1029/2000RG000095.

Remer, L. A., et al. (2005), The MODIS algorithm, products and validation, *J. Atmos. Sci.*, *62*, 947–973, doi:10.1175/JAS3385.1.

Sassen, K., P. J. DeMott, J. M. Prospero, and M. R. Poellot (2003), Saharan dust storms and indirect aerosol effects on clouds: CRYSTAL-FACE results, *Geophys. Res. Lett.*, *30*(12), 1633, doi:10.1029/2003GL017371.

Seinfeld, J. H., and S. N. Pandis (1998), *Atmospheric Chemistry and Physics: From Air Pollution to Climate Change*, Wiley, New York.

Shell, K. M., and R. C. J. Somerville (2007), Direct radiative effect of mineral dust and volcanic aerosols in a simple aerosol climate model, *J. Geophys. Res.*, *112*, D03205, doi:10.1029/2006JD007197.

Sokolik, I. N., and O. B. Toon (1996), Direct radiative forcing by anthropogenic airborne mineral aerosols, *Nature*, *381*, 681–683, doi:10.1038/381681a0.

Solmon, F., P. Y. Chuang, N. Meskhidze, and Y. Chen (2009), Acidic processing of mineral dust iron by anthropogenic compounds over the north Pacific Ocean, *J. Geophys. Res.*, *114*, D02305, doi:10.1029/2008JD010417.

Solomos, S., G. Kallos, J. Kushta, M. Astitha, C. Tremback, A. Nenes, and Z. Levin (2011), An integrated modeling study on the effects of mineral dust and sea salt particles on clouds and precipitation, *Atmos. Chem. Phys.*, *11*, 873–892, doi:10.5194/acp-11-873-2011.

Sun, J., M. Zhang, and T. Liu (2001), Spatial and temporal characteristics of dust storms in China and its surrounding regions, 1960–1999: Relations to source area and climate, *J. Geophys. Res.*, *106*, 10,325–10,333, doi:10.1029/2000JD900665.

Tanré, D., Y. J. Kaufman, M. Herman, and S. Mattoo (1997), Remote sensing of aerosol properties over oceans using the MODIS/EOS spectral radiances, *J. Geophys. Res.*, *102*, 16,971–16,988, doi:10.1029/96JD03437.

Tegen, I., and A. A. Lacis (1996), Modeling of particle size distribution and its influence on the radiative properties of mineral dust aerosol, *J. Geophys. Res.*, *101*, 19,237–19,244, doi:10.1029/95JD03610.

Tegen, I., A. A. Lacis, and I. Fung (1996), The influence of mineral aerosol from disturbed soils on the global radiation budget, *Nature*, *380*, 419–422, doi:10.1038/380419a0.

Tegen, I., P. Hollrig, M. Chin, I. Fung, D. J. Jacob, and J. Penner (1997), Contribution of different aerosol species to the global aerosol extinction optical thickness: Estimates from model results, *J. Geophys. Res.*, *102*, 23,895–23,915, doi:10.1029/97JD01864.

Tegen, I., S. P. Harrison, K. Kohfeld, I. C. Prentice, M. Coe, and M. Heimann (2002), Impact of vegetation and preferential source areas on global dust aerosol: Results from a model study, *J. Geophys. Res.*, *107*(D21), 4576, doi:10.1029/2001JD000963.

Torres, O., P. K. Bhartia, J. R. Herman, and Z. Ahmad (1998), Derivation of aerosol properties from satellite measurements of backscattered ultraviolet radiation: Theoretical basis, *J. Geophys. Res.*, *103*, 17,099–17,110, doi:10.1029/98JD00900.

Torres, O., A. Tanskanen, B. Veihelmann, C. Ahn, R. Braak, P. K. Bhartia, P. Veefkind, and P. Levelt (2007), Aerosols and surface UV products from Ozone Monitoring Instrument observations: An overview, *J. Geophys. Res.*, *112*, D24S47, doi:10.1029/2007JD008809.

van Donkelaar, A., R. V. Martin, and R. J. Park (2006), Estimating ground-level $PM_{2.5}$ using aerosol optical depth determined from satellite remote sensing, *J. Geophys. Res.*, *111*, D21201, doi:10.1029/2005JD006996.

Vaughan, M., S. Young, D. Winker, K. Powell, A. Omar, Z. Liu, Y. Hu, and C. Hostetler (2004), Fully automated analysis of space-based lidar data: An overview of the CALIPSO retrieval algorithms and data products, *Proc. SPIE Int. Soc. Opt. Eng.*, *5575*, 16–30.

Wen, G. Y., A. Marshak, and R. F. Cahalan (2006), Impact of 3-D clouds on clear-sky reflectance and aerosol retrieval in a biomass burning region of Brazil, *IEEE Trans. Geosci. Remote Sens. Lett.*, *3*(1), 169–172, doi:10.1109/LGRS.2005.861386.

Wen, G. Y., A. Marshak, R. F. Cahalan, L. A. Remer, and R. G. Kleidman (2007), 3-D aerosol-cloud radiative interaction observed in collocated MODIS and ASTER images of cumulus cloud fields, *J. Geophys. Res.*, *112*, D13204, doi:10.1029/2006JD008267.

Winker, D. M., M. A. Vaughan, A. Omar, Y. Hu, K. A. Powell, Z. Liu, W. H. Hunt, and S. A. Young (2009), Overview of the CALIPSO mission and CALIOP data processing algorithms, *J. Atmos. Oceanic Technol.*, *26*, 2310–2323, doi:10.1175/2009JTECHA1281.1.

Wu, S., L. J. Mickley, D. J. Jacob, J. A. Logan, R. M. Yantosca, and D. Rind (2007), Why are there large differences between models in global budgets of tropospheric ozone?, *J. Geophys. Res.*, *112*, D05302, doi:10.1029/2006JD007801.

Wu, S., L. J. Mickley, E. M. Leibensperger, D. J. Jacob, D. Rind, and D. G. Streets (2008), Effects of 2000–2050 global change on ozone air quality in the United States, *J. Geophys. Res.*, *113*, D06302, doi:10.1029/2007JD008917.

Wurzler, S., T. G. Reisin, and Z. Levin (2000), Modification of mineral dust particles by cloud processing and subsequent effects on drop size distributions, *J. Geophys. Res.*, *105*, 4501–4512, doi:10.1029/1999JD900980.

Young, S., and M. Vaughan (2009), The retrieval of profiles of particulate extinction from Cloud Aerosol Lidar Infrared Pathfinder Satellite Observation (CALIPSO) data: Algorithm description, *J. Atmos. Oceanic Technol.*, *26*, 1105–1119, doi:10.1175/2008JTECHA1221.1.

Yu, H., M. Chin, D. M. Winker, A. H. Omar, Z. Liu, C. Kittaka, and T. Diehl (2010), Global view of aerosol vertical distributions from CALIPSO lidar measurements and GOCART simulations: Regional and seasonal variations, *J. Geophys. Res.*, *115*, D00H30, doi:10.1029/2009JD013364.

Zender, C. S., D. Newman, and O. Torres (2003), Spatial heterogeneity in aeolian erodibility: Uniform, topographic, geomorphic, and hydrologic hypotheses, *J. Geophys. Res.*, *108*(D17), 4543, doi:10.1029/2002JD003039.

Zhang, L., S. Gong, J. Padro, and L. Barrie (2001), A size-segregated particle dry deposition scheme for an atmospheric aerosol module, *Atmos. Environ.*, *35*(3), 549–560, doi:10.1016/S1352-2310(00)00326-5.

Zhang, J., J. S. Reid, and B. N. Holben (2005), An analysis of potential cloud artifacts in MODIS over ocean aerosol optical thickness products, *Geophys. Res. Lett.*, *32*, L15803, doi:10.1029/2005GL023254.

Corresponding author: N. Meskhidze, Marine Earth and Atmospheric Science, North Carolina State University, Raleigh, NC 27695, USA. (nmeskhidze@ncsu.edu)